phases, α and α', would be revealed.

Splitting of the Se_{3d} lines was observed, indicative of the presence of coupled and noncoupled selenium atoms. The splitting of the Se_{3d} peaks (1.2 ± 0.1 eV) is slightly less than that observed for α-P_4Se_3. The smaller splitting suggests that the difference between coupled and noncoupled selenium atoms is less distinct than in α-P_4Se_3. The binding energies and the electron densities on the noncoupled selenium atoms are approximately the same in α- and α'-P_4Se_3. The binding energy of the coupled selenium atoms in α'-P_4Se_3 is slightly lower than that in α-P_4Se_3. From this it may be concluded that the electron density on the coupled selenium atoms in α'-P_4Se_3 is slightly higher than on the coupled selenium atoms in α-P_4Se_3, implying that there is less delocalization of electrons between α'-P_4Se_3 molecules. This in turn implies that the coupling between molecules is weaker in the α' phase.

Discussion

The structure of α-P_4Se_3 can be described as consisting of layers of double-stranded helices. Each helix, lying orthogonal to the long c axis of the unit cell, is composed of intermolecularly bonded cages in which Se···Se and some P···Se contacts are important. In α'-P_4Se_3, the individual helices are retained but are no longer paired due to a different orientation for alternate helices along the c direction. This different packing has P···P and P···Se interactions separating the layers. The changes in the unit cell dimensions reflect these differences in that for the equivalent α cell ($a \times b \times {}^1/_2c$), there is an increase of 5.6% in c, a comparable decrease of 6.2% in a, and a small increase of 2.4% in b on going from α to α'. This can be interpreted as indicating a weakening of the intermolecular bonding along the c direction as the Se···Se interaction, giving rise to the double-stranded structure, is replaced by the weaker P···P interaction. There is a concomitant strengthening of the intermolecular bonding in the 001 plane. This parallels the changes observed for selenium chains in mordenite, a zeolite matrix. An EXAFS study[15] showed that the nearest Se–Se distance in selenium chains is shortened compared to the value in trigonal selenium. The covalent bond along the chain becomes stronger when coupling between adjacent chains is inhibited.

The temperature dependence of the unit cell parameters for α-P_4Se_3 is also informative about the intermolecular bonding. A comparison of the observed changes (Table IV) with those previously reported[16] for α-P_4S_3 shows that the changes in b and c are similar whereas the change in a is only about half that observed in the sulfide crystal. If this reflects stronger intermolecular bonding in the selenide, then it supports the earlier observation[4,17] of stronger intermolecular–intramolecular coupling for α-P_4Se_3 compared to α-P_4S_3.

The small but measurable differences between the lattices for α- and α'-P_4Se_3 are confirmed by the Raman and XPS spectra of the two crystals. In the case of the XPS data, it has been possible to identify the presence of two distinct types of selenium atom, differing in terms of the extent to which they are involved in strong intermolecular Se···Se bonding.

Acknowledgment. Dr. A. R. MacGibbon, Dairy Research Institute, Palmerston North, New Zealand, is thanked for help in obtaining the DSC data, and J.R.R. thanks the UGC for the award of a postgraduate scholarship, during the tenure of which this work was completed.

Registry No. P_4Se_3, 1314-86-9; P_4S_3, 1314-85-8.

Supplementary Material Available: A textual summary of the structural determination and tables of atomic fractional coordinates, anisotropic temperature factors, bond lengths and angles, and selected nonbonded distances for α-P_4Se_3 and anisotropic temperature factors for α'-P_4Se_3 (6 pages); listings of structure factors for α-P_4Se_3 and α'-P_4Se_3 (11 pages). Ordering information is given on any current masthead page.

(15) Tamura, K.; Hosokawa, S.; Endo, H.; Yamasaki, S.; Oyanagi, H. *J. Phys. Soc. Jpn.* **1986**, *55*, 528.

(16) Chattopadhyay, T. K.; May, W.; von Schnering, H. G.; Pawley, G. S. *Z. Kristallogr.* **1983**, *165*, 47.

(17) Burns, G. R.; Rollo, J. R. *J. Phys. Chem. Solids* **1987**, *48*, 347.

Contribution from the Department of Chemistry, Princeton University, Princeton, New Jersey 08544-1009

Nickel-Electrode-Confined $\{Ru(bipyrazine)_3[Fe(CN)_5]_n\}^{2-3n}$: An Inorganic Structural Matrix Yielding Photoinduced Multinuclear Charge-Transfer Reactivity

Carmela Hidalgo-Luangdilok and Andrew B. Bocarsly*,†

Received August 8, 1989

The complex $\{Ru(bpz)_3[Fe(CN)_5]_n\}^{2-3n}$ (where n = 1–6 and bpz ≡ bipyrazine) containing a central ruthenium(II) and an overall octahedral site symmetry can be surface-attached to a variety of electrodes via reaction with electrogenerated nickel ions. The well-defined geometry of this complex allows it to be considered as a "molecular building block" for the construction of microstructure-specific chemically derivatized interfaces. In addition to exhibiting a sophisticated interfacial structure, this class of electrodes is found to yield both photocathodic and photoanodic currents under illumination in an aqueous electrolyte. The photocurrent is found to be molecular in nature and can be explained in terms of charge-transfer quenching of a Ru(II) → bpz charge-transfer excited state by the pendant pentacyanoferrate groups. Excitation and quenching events appear to be highly localized. The sense of the photocurrent is controlled by the initial oxidation state of the surface-confined iron. Under conditions yielding a photocathodic current, the charge is eventually consumed by the reduction of dissolved O_2.

Introduction

A variety of approaches have been developed for the attachment of chromophores to electrode surfaces. Among these is the use of polymer and polyelectrolyte coatings, which can readily incorporate various ionic electroactive species such as $Ru(bpy)_3^{2+}$ (bpy = bipyridine) into their matrices.[1] Using this approach, modification of semiconductor electrode surfaces with $Ru(bpy)_3^{2+}$ in many cases has led to the observation of a photoresponse that is attributed to the quenching of the metal-to-ligand charge-transfer (MLCT) excited state of $Ru(bpy)_3^{2+*}$ by quenchers

* To whom correspondence should be addressed.
† Alfred P. Sloan Fellow, 1986–1988.

(1) (a) Oyama, N.; Anson, F. C. *J. Am. Chem. Soc.* **1979**, *101*, 739. (b) Oyama, N.; Anson, F. C. *J. Electrochem. Soc.* **1980**, *127*, 247. (c) Oyama, N.; Shimomura, K.; Shigehara, K.; Anson, F. C. *J. Electroanal. Chem. Interfacial Electrochem.* **1980**, *112*, 271. (d) Rubinstein, I.; Bard, A. J. *J. Am. Chem. Soc.* **1980**, *102*, 6641. (e) Rubinstein, I.; Bard, A. J. *J. Am. Chem. Soc.* **1981**, *103*, 5007.

0020-1669/90/1329-2894$02.50/0

present in the solution or immobilized on the surface. Recently, there have been reports of dye-sensitized photoinduced currents at metallic electrodes, where rapid energy-transfer quenching through the continuum of metal states is expected to lead to very inefficient photoinduced interfacial charge transfer.[2]

We report here the attachment of $Ru(bpz)_3^{2+}$ (bpz = 3,2',4,4'-bipyrazine) to various electrode surfaces via a cyanometalate matrix of the Prussian Blue type. The tris(bipyrazine)ruthenium(II) complex has been reported in the literature as a promising solution-based charge-transfer photocatalyst having many complementary properties with respect to the tris(bipyridine)ruthenium(II) cation.[3] The surface-confined complexes employed here involve coordination of "$Fe(CN)_5^{3-n}$" units to the bpz outer nitrogens. Such binuclear complexes were originally synthesized and characterized in solution[4] by Toma and Lever. Unlike polymer-bound chromophores, tris(bipyrazine)ruthenium(II) pentacyanoferrate complexes have a well-defined geometry that combines a charge-transfer quencher, "$Fe(CN)_5^{2-/3-n}$", and a chromophore via a covalent bond. The attachment of such systems to an electrode surface via an extended system of bridging cyanide ligands not only provides a good method for examining the spectroscopic and photochemical properties of such binuclear complexes in various oxidation states but also allows for the construction of microstructure-specific chemically derivatized interfaces based on the molecular geometry of the $\{Ru(bpz)_3[Fe(CN)_5]_n\}^{2-3n}$ complexes.

Dissolved $Ru(bpz)_3^{2+}$ no longer emits upon reaction with the pentacyanoferrates. Similarly, no photochemistry has been reported for $\{Ru(bpz)_3[Fe(CN)_5]_n\}^{2-3n}$ polynuclear complexes. Once surface confined, we find these complexes exhibit electrochemical and spectroscopic properties very similar to those of the solution species. However, a rich photochemical response is also obtained, indicative of charge-transfer interactions between the two types of metal centers. This interaction gives rise to a sustained photocurrent in the presence of appropriate electroactive solution species.

Experimental Section

The $\{Ru(bpz)_3[Fe(CN)_5]_n\}^{2-3n}$ complexes were synthesized by following the method reported by Toma et al.[4] $Ru(bpz)_3Cl_2$[5] and $Na_3[Fe(CN)_5NH_3]\cdot 3H_2O$[6] were prepared by literature methods. The bipyrazine complex, which was previously dissolved in aqueous solution, was reacted with the amminepentacyanoferrate(II) salt under an argon atmosphere. Ammonia was released from the latter upon solution, and the aquapentacyanoferrate(II) ion was formed. The species where the Ru:Fe ratio is 1:3 was first prepared in an excess amount of aquapentacyanoferrate(II) complex. To obtain a pure 1:3 species, the reaction mixture was lyophilized to concentrate it and run through a column of Sephadex G-25. To verify whether the separation from the excess aquapentacyanoferrate(II) species was achieved, 1-(4-pyridyl)pyridinium chloride hydrochloride (4-PP) (Aldrich) was used as an indicator. This ligand reacts rapidly with the aquapentacyanoferrate(II) complex to form $[Fe(CN)_5(4\text{-pyridylpyridinium})]^{2-}$, whose absorbance maximum is at 483 nm ($\epsilon_{max} = 3.80 \times 10^3\ M^{-1}\ cm^{-1}$).[7] From the absorptivity monitored at this wavelength before and after adding the ligand, the amount of unreacted $[Fe(CN)_5H_2O]^{3-}$ could be obtained. No change was detected in the absorbance at 700 nm assigned to the Fe(II) → bpz charge-transfer band during the first few minutes after adding 4-PP, independent of changes in the 483-nm region. Therefore, the 4-PP reacts specifically with $[Fe(CN)_5H_2O]^{3-}$ and does not lead to the immediate destruction of the $\{Ru(bpz)_3[Fe(CN)_5]_n\}^{2-3n}$ complex. NMR and UV-vis absorption spectroscopy of the chromatographed material confirmed the existence of the 1:3 species.[4]

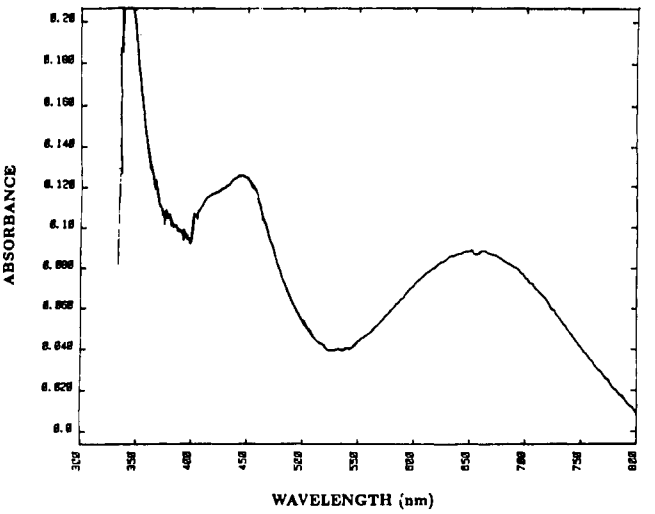

Figure 1. UV-visible absorption spectrum of a nickel-plated optically transparent SnO_2 electrode derivatized with a solution containing the 1:3 species. A blank SnO_2 glass was used as reference.

Attachment of the polynuclear complex to a nickel electrode surface was achieved by using the same approaches previously reported for $[NiFe(CN)_6]^{2-}$ attachment.[8] The nickel electrode was anodized at positive potentials (0.1–1.6 V vs SCE) for 5–15 min in a 0.005 M aqueous solution of the complex in 0.1 M $NaNO_3$. This procedure generates Ni^{2+} ions that bind to the anionic cyanometalate complex via the nitrogen end of the cyanide ligand, generating an insoluble three-dimensional inorganic polymer. Typical coverages ranged from 1×10^{-9} to 5×10^{-8} mol/cm^2 on the electrode surface. Derivatization on SnO_2 (PPG) as well as on Pt electrodes was carried out by first electroplating a thin nickel layer onto the electrodes. The electrode was placed in aqueous 0.1 M $NaNO_3$ electrolyte containing $\sim 1 \times 10^{-3}$ M nickel sulfate and stepped from −0.3 to −1.0 V vs SCE. After ~30 s at −1.0 V vs SCE, the electrode was linearly scanned (100 mV/s) to 0.0 V. This process was repeated until a reproducible i–E plot was obtained. Nickel metal was deposited by holding the electrode at −1.0 V for times varying from 5 to 10 min.

All electrochemical experiments were carried out in a standard three-electrode cell employing an SCE reference electrode and a large-area platinum counter electrode. A 1 M concentration of supporting electrolyte was used unless stated otherwise. Cyclic voltammograms were recorded directly on a Houston Instruments 2000 X-Y recorder using a PAR 173 or 174A potentiostat/PAR 175 universal programmer.

Absorption spectra were obtained on a Hewlett-Packard 8450A Diode Array spectrophotometer. Diffuse-reflectance FTIR spectroscopy was performed by using a Digilab FTS.20C spectrometer with a diffuse-reflectance attachment. Spectra were referenced against unmodified electrodes.

Monochromatic light at 488 nm was provided by a Spectra Physics Model 164 argon ion laser. To obtain the photoaction spectra, the light source was a PTI 150-W xenon compact arc lamp combined with a high-throughput $^1/_4$-m monochromator The spectra were corrected for the spectral distribution of the light source and the monochromator.

Results and Discussion

Surface Characterization. Reaction of a nickel-plated, optically transparent SnO_2 electrode with the 1:3 species gives rise to a surface yielding the UV-visible absorption spectrum shown in Figure 1. This spectrum is similar to the solution absorption spectrum reported by Toma and Lever that has a Ru(II) → bpz(π^*) charge-transfer absorption band at 445 nm and a Fe(II) → bpz(π^*) charge-transfer absorption at 700 nm. The Fe(II)

(2) (a) Abruna, H. D.; Denisevich, P.; Umana, M.; Meyer, T. J.; Murray, R. W. *J. Am. Chem. Soc.* **1981**, *103*, 1. (b) Samuels, G. J.; Meyer, T. J. *J. Am. Chem. Soc.* **1981**, *103*, 307. (c) Westmoreland, T. D.; Calvert, J. M.; Murray, R. W.; Meyer, T. J. *J. Chem. Soc., Chem. Commun.* **1983**, 65. (d) Hupp, J. T.; Otruba, J. P.; Parus, S. J.; Meyer, T. J. *J. Electroanal. Chem. Interfacial Electrochem.* **1985**, *190*, 287. (e) Hupp, J. T.; Meyer, T. J. *J. Electroanal. Chem. Interfacial Electrochem.* **1987**, *224*, 59. (f) Margerum, L. D.; Meyer, T. J.; Murray, R. W. *J. Electroanal. Chem. Interfacial Electrochem.* **1983**, *149*, 279. (g) Yamamura, T.; Umezawa, Y. *J. Chem. Soc., Dalton Trans.* **1982**, 1977. (h) Keishman, M.; Zhang, X.; Bard, A. J. *J. Am. Chem. Soc.* **1984**, *106*, 737. (i) Haas, O.; Vox, J. G. *J. Electroanal. Chem. Interfacial Electrochem.* **1980**, *113*, 139. (j) Oyama, N.; Yamaguchi, S.; Kaneko, M.; Yamada, A. *J. Electroanal. Chem. Interfacial Electrochem.* **1982**, *139*, 215. (k) Kaneko, M.; Yamada, A. *Electrochim. Acta* **1986**, *31*, 273.
(3) (a) Kalyansundaram, K. *Coord. Chem. Rev.* **1979**, *46*, 159. (b) Sutin, N.; Crentz, C. *Pure Appl. Chem.* **1980**, *52*, 2717.
(4) Toma, H. E.; Lever, A. B. P. *Inorg. Chem.* **1986**, *25*, 176.
(5) Crutchley, R. J.; Lever, A. B. P. *Inorg. Chem.* **1982**, *21*, 2276.
(6) Brauer, G. *Handbook of Preparative Inorganic Chemistry*, 2nd ed.; Academic Press: New York, 1965; Vol. 2, p 1511.
(7) Toma, H. E.; Malin, J. M. *Inorg. Chem.* **1973**, *12*, 1039.
(8) Sinha, S.; Humphrey, B. D.; Bocarsly, A. B. *Inorg. Chem.* **1984**, *23*, 203.

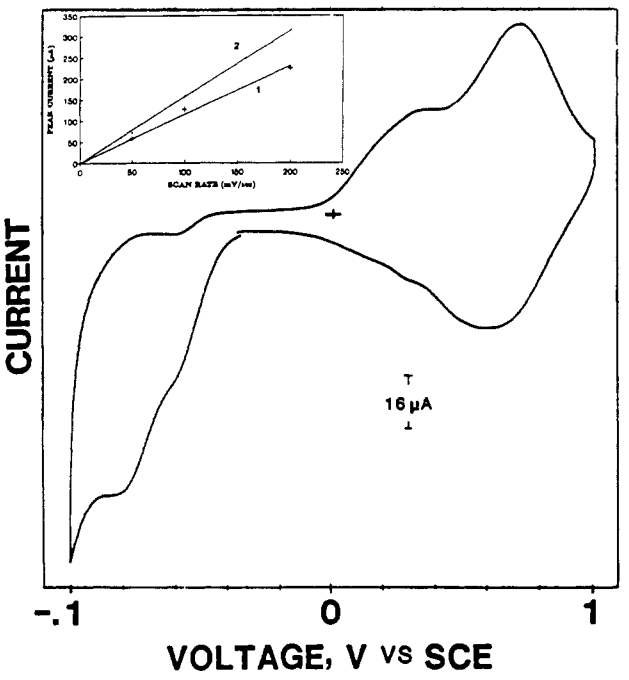

Figure 2. Typical cyclic voltammogram of electrodes modified with a solution containing the 1:3 species. This was done in 1 M $NaNO_3$ with a scan rate of 100 mV/s. The inset shows the scan rate dependence of the anodic peak currents of the two $Fe^{2+/3+}$ waves: (1) lower oxidation wave; (2) higher oxidation wave.

→ bpz(π^*) band is found to be blue shifted by ~35 nm to a wavelength of 665 nm, consistent with Ni^{2+} metalation of the cyanide ligands.[9] Within the context of a one-electron molecular orbital scheme this assignment places the dπ Fe(II) orbitals ~0.9 eV above the dπ Ru(II) orbitals.

With the use of a derivatizing solution initially containing the 1:3 species, the modified surfaces obtained exhibited two cyclic voltammetric waves at positive potentials. On nickel metal modified electrodes in 1 M $NaNO_3$ aqueous electrolyte, $E_{1/2}$ values of +0.22 and +0.56 V vs SCE were obtained (Figure 2). By analogy with surface-confined $[NiFe(CN)_6]^{2-/-}$, the two cyclic voltammetric waves are assigned to the $Fe^{2+/3+}$ oxidation and the dual wave pattern is attributed to the existence of two distinct chemical species on the electrode surface. The peak currents of both oxidation waves were linearly dependent on scan rate up to 200 mV/s, the maximum ramp rate employed. The more positive $E_{1/2}$ value is similar to that reported by Toma and Lever[4] ($E_{1/2}$ ~ 0.7 vs NHE) for species having a ruthenium:iron ratio of 1:2 or greater. Toma also reported that the 1:1 Ru:Fe species showed a negative shift in redox potential to 0.6 V vs NHE. By analogy with this potential shift, we therefore assign the more negative set of cyclic voltammetric waves to a surface-confined 1:1 species. This assignment is supported by the spectroscopy discussed in the following paragraphs. The difference in potential between the 1:1 and higher ratio species is larger than that observed in solution (300 mV compared to 100 mV reported by Toma and Lever[4]). Toma points out that the redox potential of the solution species may be affected by chemisorption onto a carbon electrode.[4] Thus, the shift in redox potential observed when the complex is derivatized onto a nickel electrode may simply be an exaggeration of this chemisorption effect. Alternatively, these shifts in $E_{1/2}$ may result from chemical changes associated with the generation of nickel-capped bridging cyanide ligands. On the basis of our prior studies of surface confined $[NiFe(CN)_6]^{2-/-}$, we expect interfacial structures of the type under discussion to yield shifts in $E_{1/2}$ that are associated with the exact solid-state structure adopted by the surface layer.[8]

(9) Previous studies on pH effects on $Fe(CN)_5L^{n-}$ (e.g., for L = methylpyrazine) complexes have reported a blue shift in the Fe → L MLCT band at lower pH due to protonation of the cyanide ligands.[7]

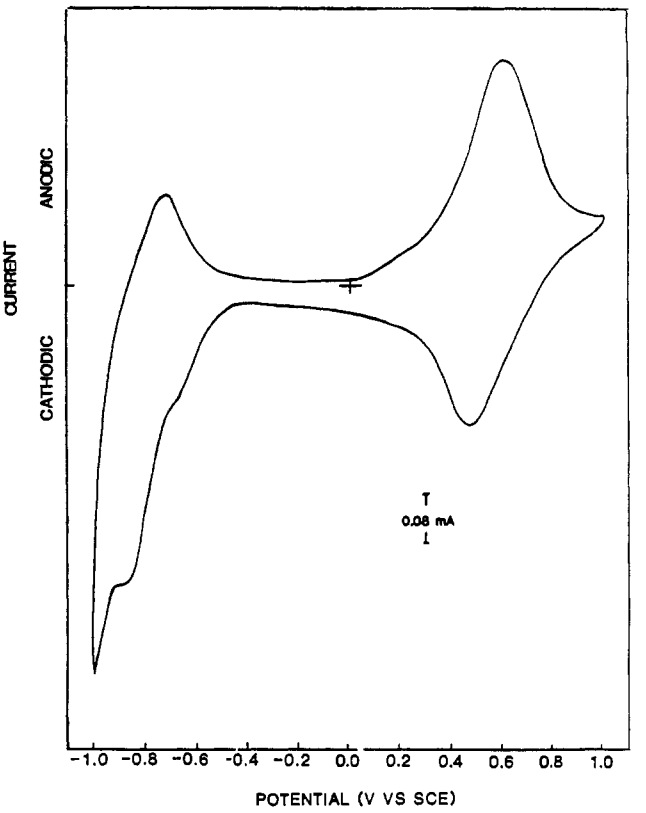

Figure 3. Cyclic voltammogram of a nickel electrode modified with a reaction solution containing the 1:3 species where an excess amount of $Ru(bpz)_3^{2+}$ was added. An electrolyte of 1 M $NaNO_3$ and a scan rate of 100 mV/s were employed.

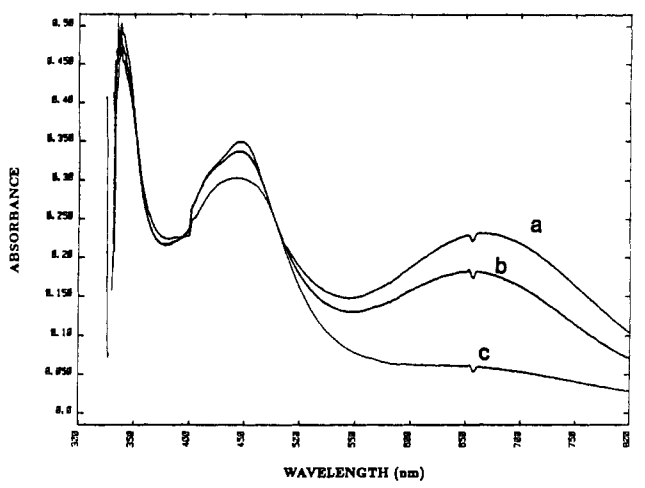

Figure 4. In situ UV–visible absorption spectra taken as a function of electrode potential (V vs SCE): (a) 0 V; (b) 0.54 V; (c) 0.92 V. This was done by using a derivatized SnO_2 electrode scanned in 1 M $NaNO_3$.

Addition of an excess amount of free $Ru(bpz)_3^{2+}$ to the derivatizing solution produced electrodes exhibiting just one oxidation wave, as shown in Figure 3 ($E_{1/2}$ = +0.56 V vs SCE). Similarly, the peak current was found to be linearly dependent on scan rate, indicating nondiffusive behavior, as expected for an electrode-confined species.

In situ UV–visible absorption spectra taken as a function of electrode potential showed that the 665-nm band decreases as the electrode potential is moved positive through the region of the cyclic voltammetric waves (Figure 4). This is consistent with oxidation of the Fe(II) centers. For electrodes showing only one oxidation wave, the amount of charge passed was found to be inversely proportional to the absorbance at 665 nm (Figure 5a). Since Toma and Lever[4] have reported different molar extinction coefficients (for the Fe(II) → bpz(π^*) MLCT band) for the

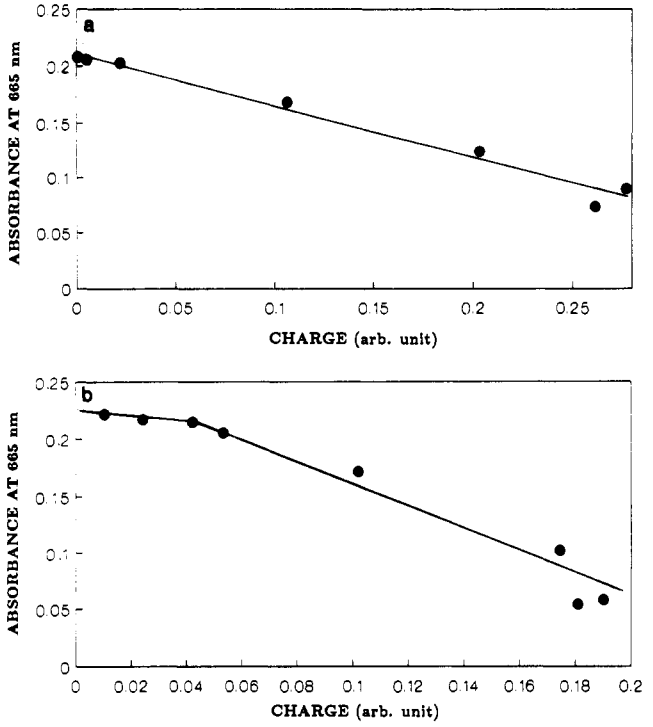

Figure 5. Plots of charge versus absorbance at 665 nm for (a) electrodes showing only one $Fe^{2+/3+}$ oxidation wave and (b) electrodes showing two cyclic voltammetric events.

various $\{Ru(bpz)_3[Fe(CN)_5]_n\}^{2-3n}$ complexes, this finding suggests the existence of only one species on the electrode surface. UV–visible spectroscopic analysis of solutions containing a complex that had been exhaustively stripped off an electrode (which yielded only one set of cyclic voltammetric peaks) by using 1 M NaOH indicates that the surface derivative is best described as $\{Ni^{II}_xRu(bpz)_3[Fe(CN)_5]_2\}^{2x-4}$. For surfaces showing two cyclic peaks, the absorbance versus charge plot (Figure 5b) is best fit as the sum of two linear plots consistent with the presence of exactly two surface species. Comparison of the molar extinction coefficients obtained from the slope of these two linear plots to those obtained by Lever[4] indicates a mixture of the 1:1 and the 1:2 species, with the former giving rise to the lower potential oxidation wave.

It should be noted that the color of these surfaces at 0 V vs SCE is green due to the 665-nm band. Removal of this absorption by oxidation of the Fe(II) centers generates a bright orange surface due to the 445-nm Ru(II) → bpz(π^*) transition. The surface is therefore electrochromic; the shift between these two color states is found to be reversible, consistent with the cyclic voltammetric results.

One feature that is curiously lacking in the spectroelectrochemistry of these derivatized surfaces is the presence of an intervalent charge-transfer band in the visible or near-IR portion of the spectrum when the iron sites are in the +3 oxidation state. Our inability to observe such a transition for the electrode-confined material led to a spectroscopic study of the binuclear complexes in solution. There again, in the spectral range 200–1800 nm, no feature associated with a Ru(II) → Fe(III) intervalent charge-transfer band could be identified. Any of a wide variety of possibilities may be acting to lower the absorptivity below our detection limit. For now, it should be noted that the absorption spectroscopy gives rise to a highly localized picture of the excited state(s).

At negative potentials, two reduction waves were observed, as shown in Figure 3. The first one at −0.6 V vs SCE and the second wave at −0.85 V vs SCE are both associated with bipyrazine-centered reductions. The observed electrochemistry is similar to that reported for free $Ru(bpz)_3^{2+}$ in solution.

Convincing evidence of an intact polynuclear complex on the surface is provided by the spectroelectrochemical absorption

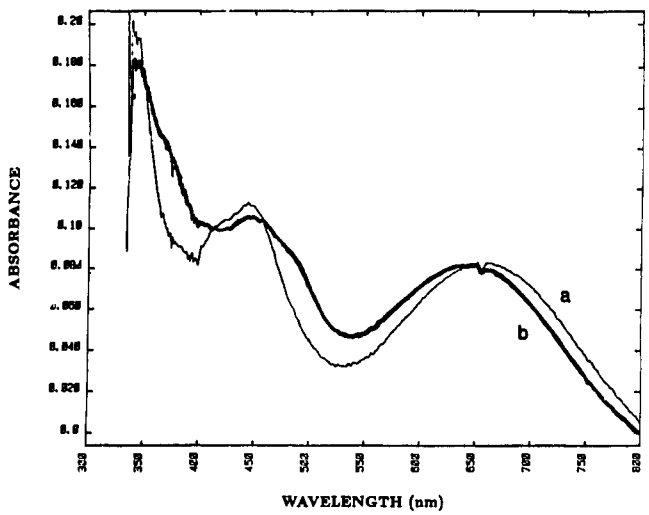

Figure 6. In situ UV–visible absorption spectra taken as a function of electrode potential: (a) 0 V; (b) −1.0 V vs SCE. Data were taken by using a derivatized SnO_2 electrode scanned in 1 M $NaNO_3$.

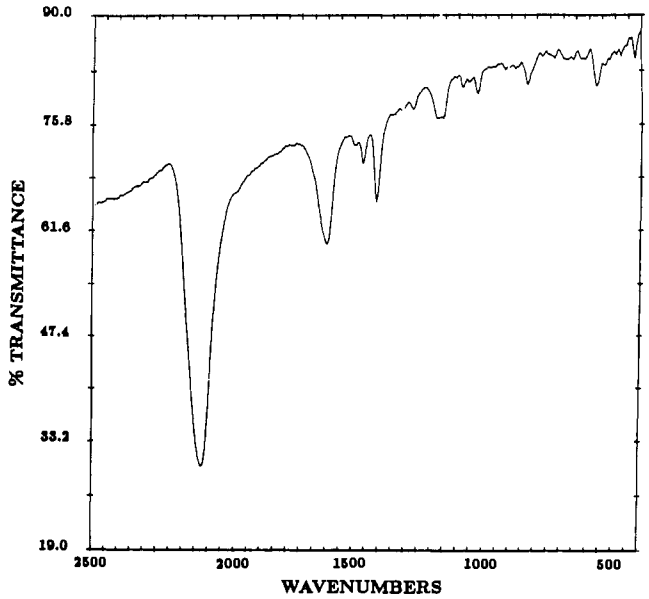

Figure 7. Typical diffuse reflectance FTIR spectrum of electrodes derivatized with both the 1:1 and 1:2 species or with just the 1:2 species. The iron complex is in the reduced state.

spectra at negative potentials (Figure 6). At −1.0 V, the absorption spectrum generated in the 400–600-nm region is the characteristic spectrum observed for a Ru(I) → bpz(π^*) transition;[10] simultaneously, the Fe(II) → bpz(π^*) band is observed to shift to higher energy (~500 cm^{-1}). These shifts are as expected for population of the bipyrazine π^* system; thus, the initial ruthenium-to-iron bipyrazine bridge must remain intact upon surface derivatization. The data further suggest that reduction preferentially places an electron on a nonderivatized bipyrazine, since reduction of a derivatized ligand is expected to induce a relatively large shift in the Fe(II) → bpz(π^*) transition. Toma and Lever previously suggested, on the basis of UV–visible spectroscopic evidence, that the π^* system of the bipyrazine is not significantly shifted in energy upon complexation with a pentacyanoferrate fragment.[4] The data provided here argue for a slight lowering in the bpz(π^*) energy upon complexation.

An attempt was made to surface-attach $[Ru(bpz)_3(Fe(CN)_5)_3]^{7-}$ (i.e. Ru:Fe = 1:3), but it was difficult to isolate just one species on the electrode and to obtain a transparent surface derivative on SnO_2 electrodes. The modified surfaces, however, exhibited electrochromism when cycled in aqueous electrolytes

(10) Crutchley, R. J.; Lever, A. B. P. *J. Am. Chem. Soc.* **1980**, *102*, 7129.

Table I. X-ray Diffraction Powder Data from an Intact Derivatized Electrode Surface[a]

2θ, deg	Miller indices[b]	2θ, deg	Miller indices[b]
19	(200)	29	(310)
23.5	(211)	35.5	(400)
26	(220)		

[a] These data were obtained by using a Phillips 120458/3 water-cooled diffractometer with a Type PN 3253/00 Cu anode operating at 40 keV and 20 mA. [b] Assignments were made by assuming a cubic crystal structure.

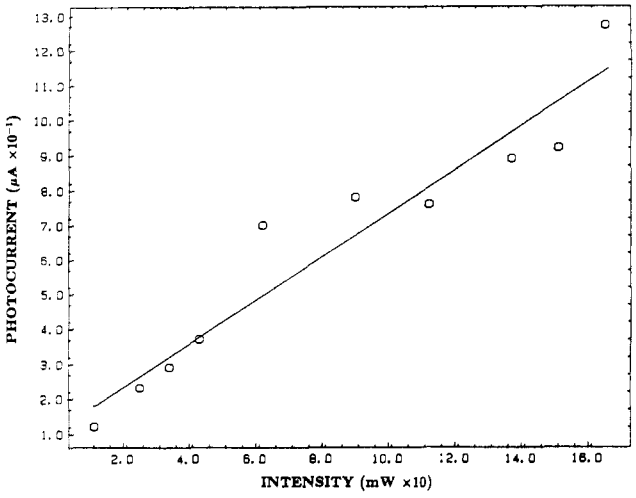

Figure 8. Cathodic photocurrent as a function of incident light intensity (488 nm). The electrode potential was held at 0 V vs SCE in 1 M $NaNO_3$ aqueous electrolyte. An active electrode surface area of ~0.1 cm^{-1} was employed.

and appeared more stable than those interfaces having derivatives with lower ratios of Ru:Fe.

There is no difference between the diffuse-reflectance FTIR spectra of electrodes with both the 1:1 and 1:2 species or with just the 1:2 species. A single CN stretching vibration band at ~2075 cm^{-1} was observed. Also present were the vibration frequencies of the bipyrazine ligand in the 650–1600-cm^{-1} region (Figure 7). Holding the electrode potential ≥0.8 V vs SCE produced a broad band centered at ~2140 cm^{-1}. This is expected since oxidation to a Fe(III) species decreases the electron density in the π-back-bonding molecular orbitals associated with the iron-to-cyanide vibration.[8] Diffuse-reflectance FTIR spectra of electrodes derivatized with higher Ru:Fe ratios showed at least two cyanide stretching vibration bands. This result is similar to the FTIR results reported for other $NiFe(CN)_5L$ surface derivatives[8,11] suggesting that electrodes derivatized with the 1:1 and 1:2 species have mostly bridged CN^- ligands.

X-ray diffraction patterns taken of these derivatized electrodes (see Table I) are consistent with a cubic symmetry and, thus, octahedral geometry about the metal centers (i.e. Ni, Fe, and Ru) on the average. Under a polarizing microscope no birefringence was observed, indicating an isometric structure consistent with cubic symmetry.[12]

Interfacial Photoresponse. No sustained current is observed if an electrode having surface irons in the +2 oxidation states is held at 0 V vs SCE in 1 M $NaNO_3$ aqueous electrolyte. However, irradiation of such an electrode–electrolyte interface with 488-nm light leads to a sustained photocathodic current, which is found to be proportional to the incident light intensity as well as to the area of illumination (Figure 8). The quantum yield for electron formation at 488 nm is calculated to be 3×10^{-5}. The photoaction spectrum observed at 0 V vs SCE applied potential, shown in

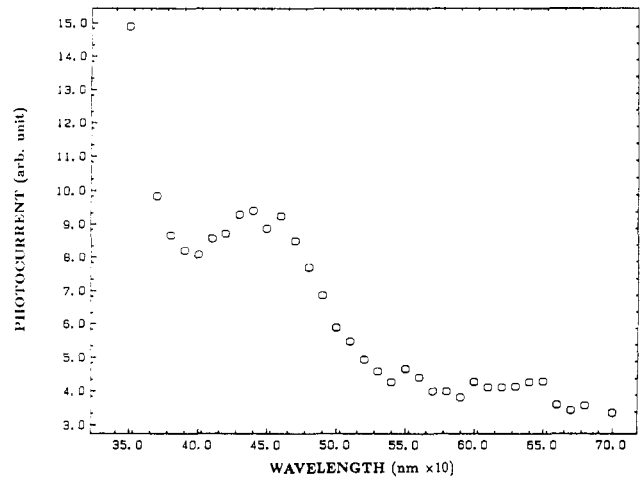

Figure 9. Photoaction spectrum of the cathodic photocurrent generated at 0 V vs SCE.

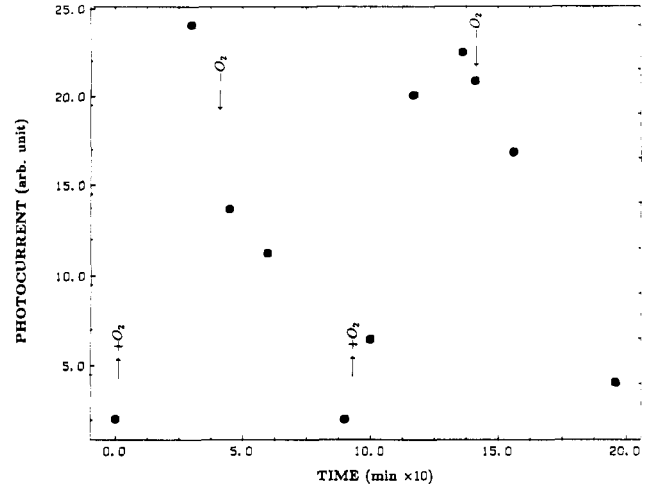

Figure 10. Dependence of the cathodic photocurrent on the presence of oxygen. Prior to the measurement, the electrode was purged in a stream of argon for several hours. The arrows indicate addition of O_2 to the argon-purged cell.

Figure 9, closely resembles the absorption spectrum of the surface derivative (see Figure 1) showing both the Ru(II) → bpz(π*) MLCT and the Fe(II) → bpz(π*) bands. The quantum yield for the iron-associated process appears to be ~4 times smaller than that associated with the Ru(II) → bpz(π*) transition. As in the case of absorption spectroscopy, no evidence for an intervalent charge-transfer transition is obtained. Thus, the observed photocurrent most likely does not arise from a delocalized band-type (i.e. semiconducting) electronic structure in the derivatizing layer. Rather, photocurrent generation appears to be molecular in nature.

The photocurrent is found to be dependent on the presence of oxygen. Within the limitations of instrumental sensitivity, the photocurrent is eliminated after prolonged argon purging. Once oxygen is bubbled back into the electrolyte, the steady-state photocurrent quickly recovers (Figure 10). This suggests the ultimate receptor of the photoproduced electron is dissolved O_2. Extensive control experiments demonstrate that the photocurrent is not due to the substrate or accidental NiO formation. No photocurrent was observed with any of the substrates or NiO alone by using >400-nm irradiation even in the presence of $Ru(bpz)_3^{2+}$ or $Co(NH_3)_6^{3+}$ in the electrolyte solution.

The direction of the photocurrent is found to be dependent on the applied potential. In 1 M $NaNO_3$, potentials more positive than ca. 0.3 V vs SCE induced anodic photocurrent while potentials lower than this value induced cathodic photocurrent (Figure 11). Unlike the photocathodic current, the photoanodic current is insensitive to the presence of O_2. These observations are consistent with the conclusion drawn above that the photo-

(11) Sinha, S.; Humphrey, B. D.; Fu, E.; Bocarsly, A. B. *J. Electroanal. Chem. Interfacial Electrochem.* **1984**, *162*, 351.
(12) Hartshorne, N. H.; Stuart, A. *Crystals and the Polarizing Microscope*; American Elsevier: New York, 1970.

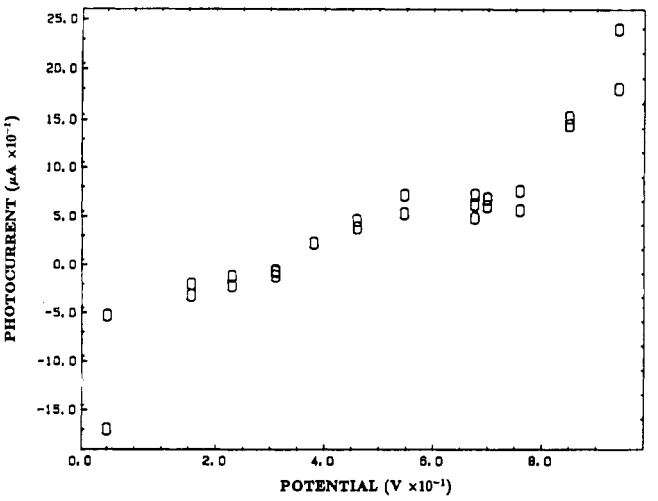

Figure 11. Change in the direction of the photocurrent as a function of applied potential in 1 M $NaNO_3$.

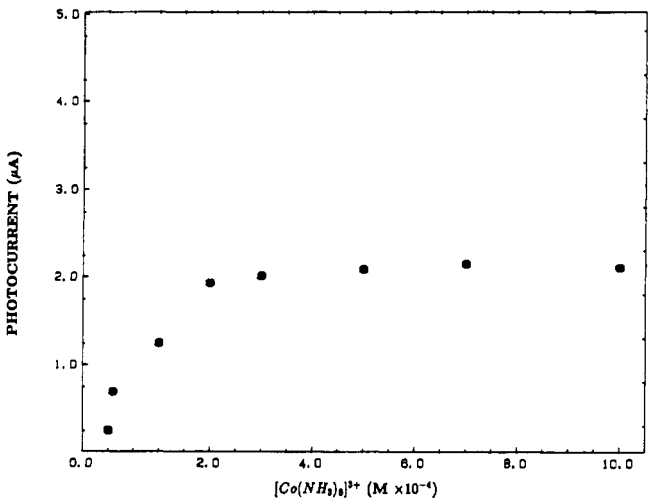

Figure 12. Magnitude of cathodic photocurrent generated as a function of the concentration of $Co(NH_3)_6^{3+}$(aq) in the electrolyte. A 400-nm-light source was used to induce the photocurrent since the cobalt complex does not absorb strongly at this wavelength. The electrolyte was stirred during the measurement, and the electrode potential was held at 0 V vs SCE.

current is not related to the generation of a semiconductor junction since a change in the sense of the current would imply the ability to switch from an n-type to a p-type interface. This is highly unlikely.

A possible mechanism to explain the observed photocathodic response under 400–500-nm irradiation at 0 V applied potential involves the reductive quenching of the $Ru(bpz)_3^{2+*}$ excited state by the "$Fe(CN)_5^{3-n}$" moiety as depicted by eqs 1–3. ΔG for reaction 1 has been calculated to be −0.89 eV.[13,14]

$$Ru(bpz)_3^{2+*} + \text{"}Fe(CN)_5^{3-n}\text{"} \rightarrow Ru(bpz)_3^{+} + \text{"}Fe(CN)_5^{2-n}\text{"} \quad (1)$$

$$\text{"}Fe(CN)_5^{2-n}\text{"} + e \rightarrow \text{"}Fe(CN)_5^{3-n}\text{"} \quad (2)$$

$$Ru(bpz)_3^{+} + \tfrac{1}{2}O_2 \rightarrow \tfrac{1}{2}HO_2^{-} + Ru(bpz)_3^{2+} \quad (3)$$

The addition of $Co(NH_3)_6^{3+}$ ($E^\circ_{1/2}$ = 0.3 V vs SCE) to the electrolyte solution enhances the cathodic photocurrent by 1 order of magnitude. The amount of enhancement is dependent on the concentration of $Co(NH_3)_6^{3+}$ added (Figure 12) as well as on stirring. If the electrolyte is unstirred, a gradual decrease in photocurrent is observed. It is interesting to note that $Co(NH_3)_5Cl^{2+}$ does not enhance the photocurrent to the same extent as $Co(NH_3)_6^{3+}$.

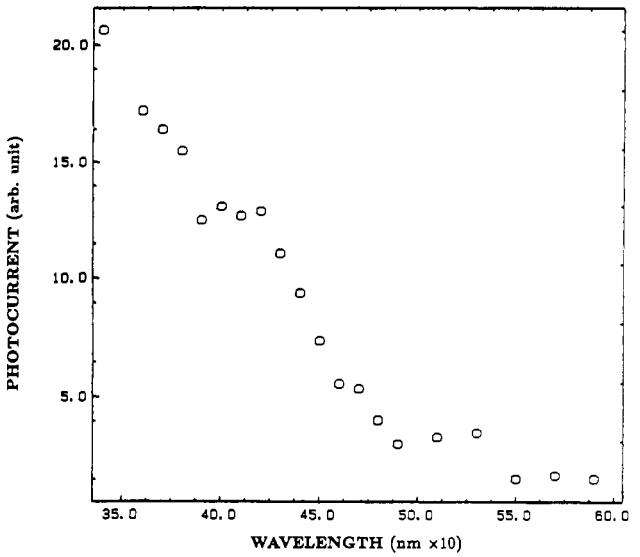

Figure 13. Photoaction spectrum of the anodic photocurrent generated at 0.77 V vs SCE.

The effect of $Co(NH_3)_6^{3+}$ or $Co(NH_3)_5Cl^{2+}$ added to the electrolyte solution on the cathodic photocurrent could be due to a direct oxidative quenching of the $Ru(bpz)_3^{2+*}$ excited state[14] by the cobalt complex. Alternatively, these electron acceptors could be reacting with a $Ru(bpz)_3^{+}$ intermediate by analogy with eq 3. Although on thermodynamic grounds either of these processes is possible, $Co(NH_3)_5Cl^{2+}$ has been reported to have a higher thermodynamic driving force than $Co(NH_3)_6^{2+}$ (by 230 mV) for the oxidative quenching of $Ru(bpz)_3^{2+*}$. In solution it has been reported that the quenching rate constant for $Ru(bpz)_3^{2+*}$ is almost 2 orders of magnitude higher for $Co(NH_3)_5Cl^{2+}$ vs $Co(NH_3)_6^{3+}$.[14] Thus, the greater enhancing effect on the cathodic photocurrent provided by $Co(NH_3)_6^{3+}$ argues for a ground-state $Ru(bpz)_3^{+}$ charge transfer and further supports eqs 1–3 as the predominant mechanism.

Likewise, the necessity for solution O_2 further supports the proposed mechanism. $Ru(bpz)_3^{+}$ is known to be oxidized by oxygen.[15] Alternatively, oxidative quenching of $Ru(bpz)_3^{2+*}$ by oxygen could generate a cathodic photocurrent. The $Ru(bpz)_3^{3+}$ formed would be converted back to $Ru(bpz)_3^{2+}$ by abstraction of an electron from the electrode. Direct electron transfer from the electrode to $Ru(bpz)_3^{2+*}$ to yield $Ru(bpz)_3^{+}$ could also be considered. However, both these mechanisms are ruled out on the basis that they cannot explain the change in the direction of the photocurrent at ≥0.3 V vs SCE.

At positive potentials (+0.3–1.0 V vs SCE), the wavelength dependence of the anodic photocurrent is similar to that obtained for the cathodic photocurrent except that the 450-nm peak is less well defined (Figure 13). This appears to be due to an increase in the photocurrent obtained around 400 nm. At these potentials, it is only the Fe that changes in oxidation state. Thus, the anodic photocurrent must be due to the occurrence of mechanisms that depend on the Fe oxidation state. Additionally, small shifts (≤20 mV difference when cycled in 1 M $NaNO_3$ vs 1 M $CsNO_3$) in the $Fe^{2+/3+}$ half-wave potential were observed depending on the electrolyte cation. We observed the onset of the change in the direction of the photocurrent to be consistent with these small shifts in the iron half-wave potential.

Since the photoaction spectra for the anodic photocurrent also suggest the involvement of $Ru(bpz)_3^{2+}$, a plausible mechanism

(13) Previously reported ground-state potential and excited-state energy for the ruthenium complex[14] have been used to calculate this value where data were not available from the experiment described here.

(14) Haga, M.; Dodsworth, E. S.; Eryavec, G.; Seymour, P.; Lever, A. B. P. *Inorg. Chem.* **1985**, *24*, 1902.

(15) Venturi, M.; Mulazzani, Q. G.; Ciano, M.; Hoffman, M. Z. *Inorg. Chem.* **1986**, *25*, 4493.

to explain the effect of the oxidation state on the photocurrent is by way of eqs 4 and 5. Note that eqs 4 and 5 do not require

$$Ru(bpz)_3^{2+*} + \text{"}Fe(CN)_5^{2-n}\text{"} \rightarrow Ru(bpz)_3^{3+} + \text{"}Fe(CN)_5^{3-n}\text{"} \quad (4)$$

$$\text{"}Fe(CN)_5^{3-n}\text{"} - e \rightarrow \text{"}Fe(CN)_5^{2-n}\text{"} \quad (5)$$

an interaction with dissolved O_2 as is experimentally observed. Oxidative quenching of the $Ru(bpz)_3^{2+*}$ excited state by the "$Fe(CN)_5^{2-n}$" complex is found to be thermodynamically favorable ($\Delta G = -0.82$ eV).[13] However, unlike the cathodic photocurrent observed at 0 V vs SCE, contributions from "$Fe(CN)_5^{2-n}$" alone to the generation of the anodic photocurrent cannot be ruled out. Anodic photocurrent has been observed during irradiation of pure $[NiFe(CN)_6]^{3-}$-modified electrodes at positive potentials. This is consistent with the photoaction spectra obtained. $[NiFe(CN)_6]^{3-}$ has previously been reported to have a strong absorbance peak centered around 400 nm.[16] Thus, the photoanodic action spectrum shown in Figure 13 can be best understood in terms of the addition of two photogalvanic processes. The response initiated by irradiation in the 300–400-nm spectral region appears associated with a $[NiFe(CN)_x]^{n-}$ species and remains uncharacterized in the present study. The response to irradiation in the 450–600-nm region involves the $\{Ru(bpz)_3[Fe(CN)_5]_n\}^{2-3n}$ complex undergoing excitation followed by anodic quenching by the cyanoferrate moiety as described in eqs 4 and 5. The possibility of a synergistic interaction between these two mechanisms cannot be ruled out. The cyanometalate-associated photochemistry is the subject of present investigations and will be reported on in the future.

Conclusion

Unlike the prior reports of photocurrent derived from $Ru(bpy)_3^{2+}$-modified electrodes, the observation of a photocurrent in the present case is unexpected due to the large number of nonproductive quenching pathways and back-reaction channels presumed available to the excited state. For many of the previously reported $Ru(bpy)_3^{2+}$ surface derivatives, electron–hole recombination or excited-state deactivation via interaction with the metal-electrode continuum of states is to some extent mitigated by the presence of an insulating polymer matrix. Likewise, deactivation or nonproductive quenching processes of a bimolecular type involving nearest-neighbor ruthenium sites are limited by the presence of an inert organic polymer matrix. Surface complexation of $\{Ru(bpz)_3[Fe(CN)_5]_n\}^{2-3n}$ does not generate an inert charge-transfer matrix. Rather, the matrix material is the photoactive element. That a photocurrent is observed indicates that charge collection at the electrode proceeds at a rate which in part precludes back-reaction processes. Such is not the case for soluble $\{Ru(bpz)_3[Fe(CN)_5]_n\}^{2-3n}$. Thus, immobilization of these binuclear complexes on the electrode surface leads to reactivity patterns that are not available in solution. Since this reactivity cannot be explained in terms of the physical separation of reaction centers by the surface immobilization process, it would appear that productive chemistry is achieved by the solid-state nature of the molecules on the electrode surface.

A simple one-electron molecular orbital scheme gives insight to the existence and directional nature of the photocurrent. In addition, the model shown in Scheme I can be used to rationalize the molecular (localized) nature of the charge-transfer process.

Scheme I. Reduced Complex

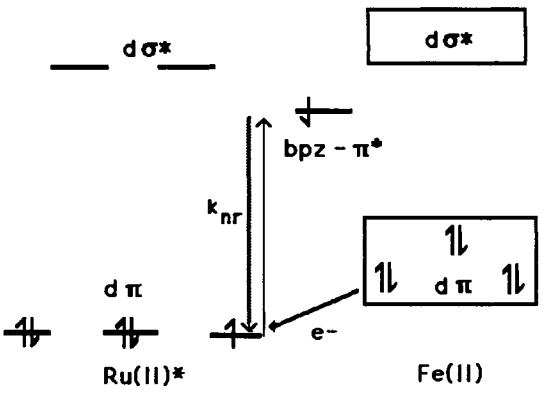

As shown in Scheme I, when both metal centers are in the reduced state, there are no available low-lying metal orbitals; thus a metal-to-metal intervalent charge-transfer transition is precluded. Irradiation into the dπ Ru(II) → bpz(π*) transition should give rise to the excited-state configuration shown. In reference again to Scheme I, it can be seen that if the excited state is sufficiently long-lived, it is possible for a dπ Fe electron to tunnel to the dπ Ru orbitals. This process is reasonable on the basis of the more positive redox potential for the oxidation of the Ru center vs the Fe center and the visible absorption spectrum of the complex (Figure 1), which indicates the dπ Fe levels are higher in energy than the dπ Ru levels. The metal-to-metal tunneling process would give rise to the chemistry outlined in reactions 1–3 at negative potentials. Irradiation into the dπ Fe → bpz(π*) transition produces an electron configuration about the Ru center that is very similar to irradiation into the dπ Ru → bpz(π*) transition. Thus, a photocathodic current is expected in this case also, as is observed. The 4-fold decrease in quantum yield observed for this transition when compared to the chemistry observed with 450-nm irradiation is consistent with previous observations that the excited-state lifetimes of iron diimine complexes are significantly shorter than those of analogous ruthenium compounds, due to fast nonradiative decay processes in the former complexes ($k_{nr} < k'_{nr}$, Scheme I).

Shifting the electrode potential positive of ~0.3 V vs SCE oxidizes the iron center, producing an electron configuration for which an intervalent metal-to-metal charge transfer is in theory possible. Irradiation into the dπ Ru → bpz(π*) transition could produce an excited state that has a high degree of dπ Fe character, if mixing between the π* system of the bipyrazine and the iron orbitals was sufficient. The lack of an experimental confirmation of such an optical transition in both the work of Toma et al. and the current study suggests that at best the coupling between the dπ metal orbitals via the bipyrazine π system is weak. Therefore, the observation of a photoanodic current is best understood in terms of a nonradiative transition between the π* bpz orbital and the dπ Fe (d^5 configuration) orbitals. This reaction channel is analogous to the oxidative quenching of ruthenium tris(diimines) by ferricyanide in solution.

Acknowledgment. This work was supported by the National Science Foundation under Grant No. CHE-8700868.

(16) Humphrey, B. D.; Sinha, S.; Bocarsly, A. B. *J. Phys. Chem.* **1984**, *88*, 736.